PHYSICAL REVIEW B **85**, 041405(R) (2012)

Far- and near-field electron beam detection of hybrid cavity-plasmonic modes in gold microholes

I. Carmeli,[1] M. A. Itskovsky,[2] Y. Kauffmann,[3] Y. Shaked,[4] S. Richter,[1] T. Maniv,[2] and H. Cohen[5]

[1]*School of Chemistry and Center for Nanoscience and Nanotechnology, Tel-Aviv University, Tel Aviv 69978, Israel*

[2]*Schulich Faculty of Chemistry, Technion-Israel Institute of Technology (IIT), 32000 Haifa, Israel*

[3]*Faculty of Material Engineering, Technion-Israel Institute of Technology (IIT), 32000 Haifa, Israel*

[4]*Physics Department, Bar-Ilan University, Ramat-Gan 52900, Israel*

[5]*Department of Chemical Research Support, The Weizmann Institute of Science, Rehovot 76100, Israel*

(Received 12 December 2011; published 24 January 2012)

Electromagnetic far- and near-field excitations of rectangular microholes in gold films are investigated by means of a focused *e* beam. Radiative cavity modes, well below the surface plasmon (SP) frequency, are detected at exceptionally large distances and are shown to be strongly enhanced at near-field regions of selected slit walls due to hybridization with metal-supported SP polaritons. The proposed enhancement mechanism of such hybridized modes, found here to preserve the cutoff frequencies and symmetry characteristics of the pure waveguide modes, sheds light on the intriguing phenomenon of extraordinary optical transmission through subwavelength apertures in metallic films.

DOI: 10.1103/PhysRevB.85.041405 PACS number(s): 73.20.Mf, 41.60.−m, 42.79.Gn, 78.66.Bz

A basic mechanism giving rise to extraordinary optical transmission (EOT) in thin metal films[1,2] concerns the breakdown of translational symmetry along subwavelength interfaces, which dramatically enhances the coupling between far-field (FF) photons and near-field (NF) surface plasmon polariton (SPP) modes.[2] While already being exploited for novel applications in, e.g., light-beam shaping devices[3] and biological molecule sensing,[4] the basic phenomenon of light coupled to SPPs in a single hole is under intense investigations (for a review, see Ref. 5). At the heart of the problem it is the electromagnetic (EM) field distribution associated with SPPs localized around the cavity walls and their interference with cavity resonances carrying the EM radiation across the hole.[6] The superior (∼0.1 nm) lateral resolution of a fast (relativistic) focused electron beam (*e* beam) at a nontouching configuration[7,8] has been exploited for spatial mapping of the NF electron energy loss (EEL) spectra of nanostructures[9,10] (for a review, see Ref. 11). Furthermore, a fast *e* beam moving in the vacuum near a dielectric medium can excite Cherenkov radiation inside the medium[12] via the evanescent tail of the near EM field. Electron beam direct excitation of EM radiation from the vacuum FF zone, involving scattering channels inside the light cone under momentum conservation breakdown along the *e*-beam direction, was also predicted,[13] but, to the best of our knowledge, so far this mechanism has not been verified experimentally. This Rapid Communication presents clear experimental evidences for this striking feature of fast *e* beams, which reveals the usually missing radiative EM field components in the entire space of metal cavities. We have found that the *e*-beam interacts with the metal through the vacuum at exceptionally long distances (∼400 nm) by exchanging photons within the light cone,[13] revealing low-energy waveguide (WG) resonances in the EEL spectrum well below the main surface plasmon (SP) peak position.

The observed WG modes appear in two distinct ways: In the FF region of the hole they are only weakly affected by SPPs, whereas in the NF regions of the slit walls their intensities are strongly enhanced by hybridizing with SPPs, preserving, however, the cutoff frequencies and symmetry characteristics of the pure WG modes. Since WG-mode resonances carry enhanced EM radiation energy across the hole, their further EELS-observed enhancement by SPPs should be related to a similar enhancement in optical transmission. For the sake of demonstration of our main findings we focus here on a relatively large (∼1 μm wide) hole, and present only briefly the results recorded from a submicrometer cavity.

EELS measurements were performed on the FEI Titan transmission electron microscope (TEM) at the Technion, using a 300-keV monochromated beam, ∼5 A in diameter, in the scanning mode. Information regarding film preparation, slit drilling, and details of the EELS measurements can be found elsewhere.[14]

Figure 1(a) shows a set of spectra, scanning the long principal axis (y) of a 900 × 4500 nm^2 slit in a free-standing gold film 200 nm thick. The appearance of low-energy signals can be easily noticed; their details are better seen after background subtraction, as shown in the main panel of Fig. 1(b). Significantly below the gold SP at 2.4 eV, peaks are observed at 0.65 and ∼1.9 eV and, with smaller intensity, also at ∼1.0 and 1.3 eV. The (seemingly noisy) spectrum shows consistently these low-energy peaks in large sets of data. Its 0.65-eV signal is attributed to a standing wave dictated by the 900-nm slit width (in the x direction). A similar set of spectra is shown in Fig. 1(c) for a 600 × 4500 nm^2 slit drilled in the same gold film, showing a pronounced low-energy signal at ∼1 eV, which is attributed to a standing wave dictated by the 600-nm slit width. To support these assignments, spectra recorded from different slits are compared in Fig. 2(a), showing the expected reciprocity between the slit width and peak position. Moreover, integer multiples of the fundamental frequency can be observed, although the second harmonic lines are relatively weak. The experimentally derived peak positions are summarized in the right-hand subcolumns of Table I. The left-hand subcolumns present the corresponding theoretical energies $\omega_m \approx c(m\pi/a)(1-\delta)$, $m = 1,2,3,\ldots$, calculated for WG resonances of infinitely long rectangular slits, where a is the slit width and $\delta = 2c/a\omega_p$, with ω_p the bulk plasmon frequency parameter, is a correction due to deviation

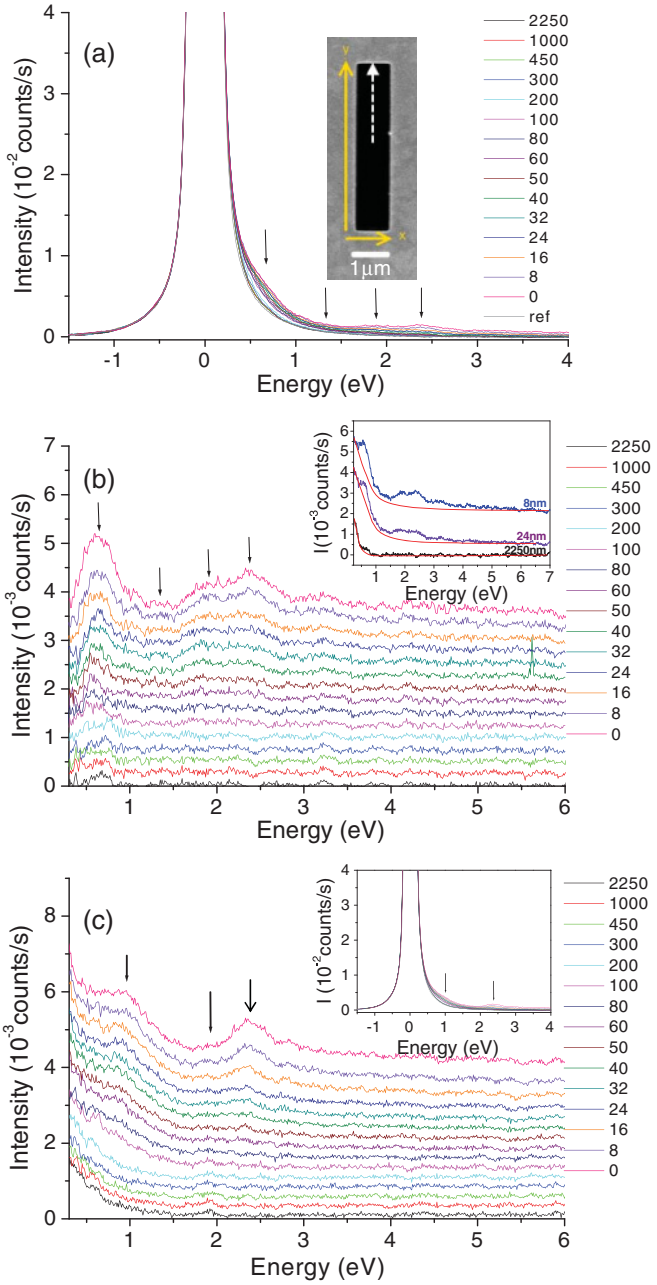

FIG. 1. (Color online) A line scan recorded along the long axis of the 900×4500 nm^2 slit shown in inset I (a) before and (b) after background subtraction. The black arrows indicate peak positions of the main resonances. The white arrow in inset I (a) indicates the scan path. Inset II (b) exemplifies the spectral shape after subtracting the reference spectrum (before the second stage of background subtraction). Spectra in (b) are shifted vertically for visual convenience. Beam positions, measured from the slit edge, are indicated in nm. (c) A line scan along the y axis of a 600×4500 nm^2 slit after background subtraction, similar to that shown in (b). The inset in (c) presents the original spectra.

from the perfect conductor (PC) boundary conditions. The good agreement found between the calculated and measured peak positions strongly supports their assignment to WG resonances. It can be shown that, despite an apparent deviation ($\delta \sim 0.1$) from the PC conditions, the even-mode fields should vanish at the slit center, a prediction which is essentially confirmed by the weak appearances of the even-mode signals in the experiment. Their nonvanishing presence, particularly that of the $m = 2$ mode in the FF region shown in Fig. 1(c), is attributed to local symmetry breaking associated with structural imperfections.

The appearance of EELS signals at distances larger than 400 nm from any of the slit edges is far beyond the distances associated with typical NF evanescent tails. It demonstrates that FF interactions from the vacuum, involving excitations within the light cone, can be realized in EELS, implying that the e beam can interact with the metal through the vacuum at exceptionally large distances due to breakdown of momentum conservation along the e-beam axis.[13] The intensity plots presented in Fig. 2(b) show a rapid signal decay from the slit edge toward the vacuum at distances of the order of 100 nm, reflecting the essentially NF nature of the interaction in this region. However, the low-energy signals remain clearly observable at much larger distances, revealing the residual FF component of the (nearly distance-independent) interaction.

To gain deeper insight into this phenomenon, we consider here a simple model of a highly focused e beam propagated in nontouching paths within an infinitely long slit in the y direction, at ascending distances from its walls. The corresponding EEL spectra are calculated by employing an extended version[13] of the method developed in Ref. 15: The effective range of the force acting on the e beam is restricted to a finite length of the order of the film thickness L while keeping the form of the self-induced EM interaction the same as in an infinite slit. The model calculation, which accounts for multiple reflections between the parallel slit walls, yields for the differential loss probability, per unit frequency ω, per unit pass length z,

$$\frac{d^2P}{d\omega dz} = \frac{e}{4\pi^2\hbar\omega L}\mathrm{Re}\left[\int_0^\infty dk_z \rho_L(k_z-\omega/v) \times \int_0^\infty dk_y E_z(x_e;k_y,k_z;\omega)\right], \quad (1)$$

where $\rho_L(k) \equiv \sin(kL)/k$, v is the electron velocity along the beam direction, and the expression for the two-dimensional (2D) Fourier transform (with wave numbers k_y,k_z) of the electric field component involved in the loss process at the position x_e of the e beam from the slit center is given by

$$E_z(x_e;k_y,k_z;\omega) = A_e\rho_L(k_z-\omega/v)[ik_z\chi_1(F_+e^{\chi_1 x_e}+F_-e^{-\chi_1 x_e}) + \gamma(1+A_+e^{\chi_1 x_e}+A_-e^{-\chi_1 x_e})]. \quad (2)$$

Here $\chi_1 \equiv \sqrt{k_y^2+k_z^2-(\omega/c)^2}$, $A_e \equiv (\frac{\pi e}{i\omega\chi_1})$, $\gamma \equiv (\omega/c)^2 - k_z^2$, $A_\pm = \alpha(\Xi_1 \pm \Xi_2)$, $\alpha = (1-\chi_2/\chi_1)e^{-\chi_1 a/2}/2$, $\Xi_1 = \cosh(\chi_1 x_e)/[\sinh(\frac{\chi_1 a}{2}) + (\frac{\chi_2}{\chi_1})\cosh(\frac{\chi_1 a}{2})]$, $\Xi_2 = \sinh(\chi_1 x_e)/[\cosh(\frac{\chi_1 a}{2}) + (\frac{\chi_2}{\chi_1})\sinh(\frac{\chi_1 a}{2})]$, and

$$F_\pm = \pm\beta\left\{\frac{\Xi_1}{\left[\varepsilon(\omega)\cosh\left(\frac{\chi_1 a}{2}\right)+\left(\frac{\chi_2}{\chi_1}\right)\sinh\left(\frac{\chi_1 a}{2}\right)\right]} \pm \frac{\Xi_2}{\left[\varepsilon(\omega)\sinh\left(\frac{\chi_1 a}{2}\right)+\left(\frac{\chi_2}{\chi_1}\right)\cosh\left(\frac{\chi_1 a}{2}\right)\right]}\right\}, \quad (3)$$

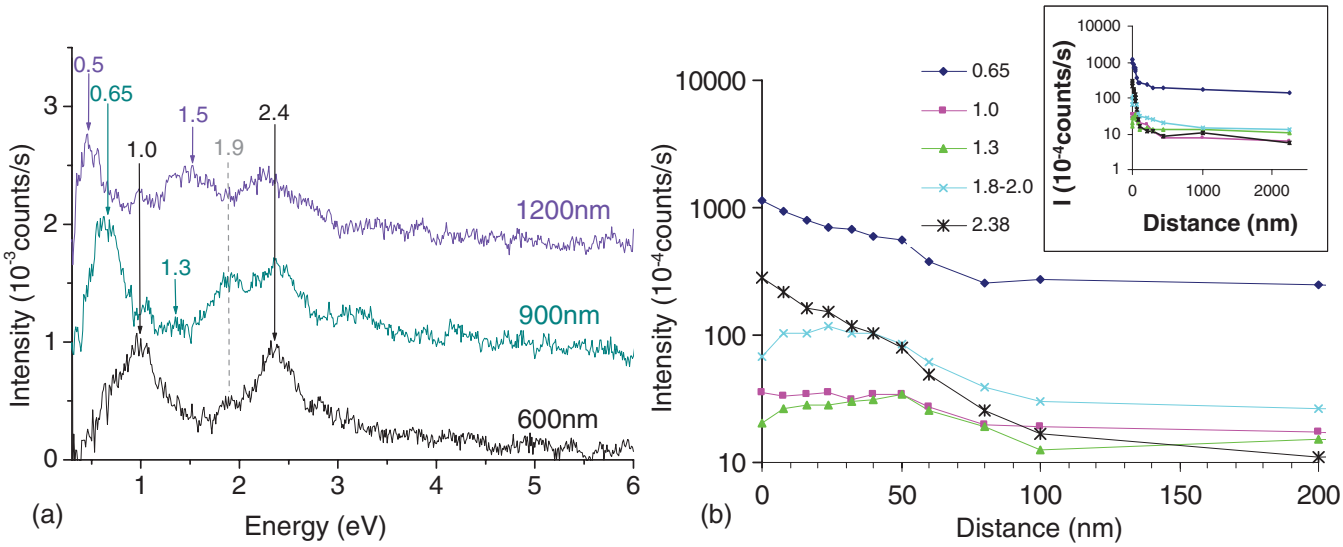

FIG. 2. (Color online) Spectra recorded at 8 nm from the narrow edge of different slits, all being 4500 nm long, with widths of 600, 900, and 1200 nm. (b) Intensity plots for selected signals in the 900 × 4500 nm^2 slit of Fig. 1(b), demonstrating the fast decay at the NF regime and the FF interaction, which takes over at long distances. The experimental error in these intensity plots is $\leqslant$30 cps.

with $\beta = ik_z(1-\varepsilon(\omega))/2\chi_1$, $\chi_2 \equiv \sqrt{k_y^2 + k_z^2 - \varepsilon(\omega)(\omega/c)^2}$, and $\varepsilon(\omega)$ the dielectric constant of the metal. The distribution function $A_e\rho_L(k_z - \omega/v)$ [see Eq. (2)], which originates in the electrical current density associated with the e beam, takes into account the finite path of active interaction with the metal. In the limit of an infinitely long cavity in the beam direction $L \to \infty$, $\rho_L(k_z - \omega/v)$ collapses to a delta function at $k_z = \omega/v$. However, for a finite L, the momentum conservation condition $k_z = \omega/v$ is not strictly satisfied and small values of k_y and k_z below ω/v become accessible, allowing wave numbers $K \equiv \sqrt{k_y^2 + k_z^2} < \omega/c$ within the light cone (i.e., with purely imaginary χ_1) to reach resonant conditions of the coefficients $A_\pm$ and $F_\pm$ [see Eqs. (3) and (2), respectively]. Note that these WG resonances and the SPPs propagating on the $x = 0,a$ walls arise from poles of the coefficients $A_\pm$ and $F_\pm$. Their interference leads to Fano-shaped resonances (see the inset to Fig. 3).

Figure 3 shows the calculated loss probability, based on Eqs. (1)–(3) for a 300-keV e beam inside a slit of width $a = 900$ nm at a distance of 400 nm from a slit edge for various values of film thickness $2L$. At this distance the gold SP resonance at 2.4 eV is fully suppressed due to its mainly non-radiative nature. On the other hand, radiative modes as the first two odd WG resonances, with thresholds at 0.65 and 1.96 eV, dominate the spectra. The inset to Fig. 3 shows the distribution of loss probability at $x_e = 300$ nm, Eq. (2), integrated over k_y, as a function of the longitudinal wave number k_z, for the three lowest WG frequencies. A typical Fano line shape, similar to EOT resonances[16,17] (with tails extended toward longer wavelengths), is seen to be located well within the light cone.

An interesting finding arising from our experimental data is the apparently selective NF enhancement of low-energy peaks with respect to the different slit edges: The enhancement is restricted to those edges that are parallel to the direction of the standing wave (the x axis). Figure 4 (bottom panel) presents spectra taken at 8 nm from each of the two perpendicular walls of a 900 × 4500 nm^2 slit. Enhancement of the fundamental and

TABLE I. Experimentally derived peak positions (right-hand subcolumns) and the corresponding theoretical energies (left-hand subcolumns).

a (nm)	ω_1 (eV)		ω_2 (eV)		ω_3 (eV)	
900	0.65	0.65	1.30	1.30	1.96	1.90
600	0.98	0.95	1.96	1.90		
1200	0.49	0.50	0.98	1.00	1.46	1.50

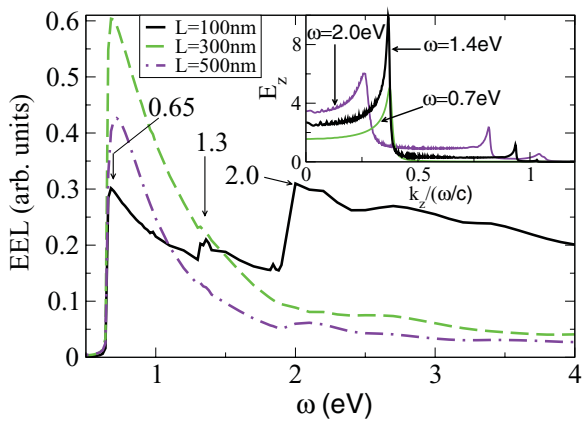

FIG. 3. (Color online) Calculated EEL spectra of a beam positioned 400 nm from the edge of a slit 900 nm wide and infinitely long, for different values of the gold film thickness ($2L$). Arrows indicate WG resonance positions. Note the sharp suppression of the high harmonics for increasing film thickness, beyond 200 nm, and the robustness of the fundamental for thicknesses up to 1000 nm. The inset shows $\int dk_y E_z(x_e;k_y,k_z;\omega)$, at $x_e = 300$ nm, as a function of k_z for the three lowest WG frequencies shown in the main figure.

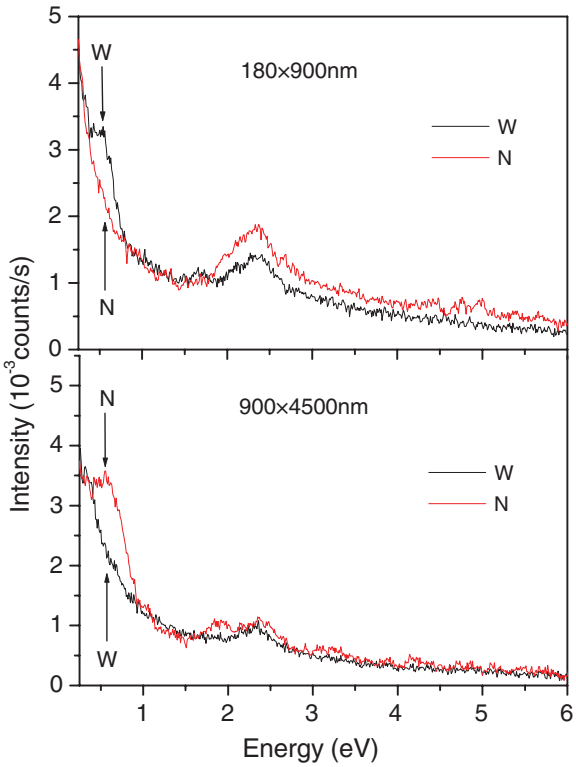

FIG. 4. (Color online) Comparison between spectra recorded at 8 nm from the narrow (N, red/gray) and wide (W, black) edges of large, 900 × 4500 nm^2 (bottom) and of small, 180 × 900 nm^2 (top), slits, showing enhanced intensities near the 900-nm-wide slit wall in both cases.

third harmonics (but not the SP at 2.4 eV) appears selectively near the short edge, i.e., the wall parallel to the (900 nm related) standing-wave direction. With a smaller slit, 180 × 900 nm^2, one finds similar NF enhancement near the long edge only, i.e., again the edge parallel to the associated standing waves.

These results contrast to the fact that the effective electric field component E_z of the corresponding WG resonances is strongly suppressed at the almost perfectly conducting walls. However, WG-SPP hybridization consisting of SPPs trapped between the $x = 0,a$ walls at $y = 0$ or b can explain our findings. The resulting standing waves have resonant WG features at the appropriate cutoff frequencies, whereas termination of the slit walls at the outer (top and bottom) film faces provides the required large E_z component via mixing with SPPs propagating on those film faces.[16] Notably, the selective NF enhancement observed here is consistent with the polarization effect reported for optical measurements under polarized light,[2] where enhanced transmission correlates with the field component (E_y in our case) perpendicular to the specific slit walls supporting the SPPs. The short range (∼100 nm ≪ 900 nm) of the NF interaction, seen in Fig. 2(b), is explained as arising from the sharp spatial rotation, as a function of y, of the electric field vector around the rims of the slit: $\mathbf{E}^{\text{face}} \sim E\hat{z} \rightarrow E\hat{y} \sim \mathbf{E}^{\text{wall}}$. A relatively large sector of the e-beam path inside the slit is exposed to this rotation due to the small (200-nm) gold film thickness. This hybridization scenario is reminiscent of the excitation mechanism of localized surface plasmon resonances, which was shown in Ref. 16 to be associated with enhanced optical transmission through an isolated nanohole.

Hybridization of low-lying WG modes with SPs also accounts for the observed EEL signals in the case of smaller (e.g., the 900 × 180 nm^2 in Fig. 4) slits, although apparent differences arise due to the small width along the y axis. Here the low-cutoff TM energy [TM(1,1)] of an ideal 2D rectangular slit with $b = 180$ nm should be considerably higher than the observed low-energy peaks [see, e.g., Fig. 4(a)], whereas the low-lying TE(1,0) WG mode, with energy that fits the experimental data, can only weakly couple to the e beam due to its null E_z field component. However, as shown recently,[18] SP oscillations on the wide slit walls, which are strongly coupled via their slowly decaying evanescent tails, should drastically modify the low-energy WG activity, introducing a new low-lying TM-like mode with a significant E_z field component near the wide slit walls.

In summary, direct radiative e-beam excitation of WG-like modes propagating in an isolated slit in a thin gold film was observed at extremely large distances of the e beam from any of the slit edges. The corresponding long-range e-beam metal interaction, involving EM excitation within the light cone, reveals WG resonances with energies well below the SP resonance of the metal. The focused e beam offers superior scanning resolution across the FF and NF regimes of the hole, providing information on both the WG and the surrounding metal-supported SPP excitations. Pronounced hybridization in the NF region between cavity and *selected* plasmonic modes strongly enhances their EEL intensities, while preserving the energy and major symmetry characteristics of ideal WG modes. This hybrid WG-SPP enhancement mechanism is essentially similar to the model of coupled surface and cavity resonances shown recently in many theoretical studies to yield EOT of light through subwavelength apertures.[5,6]

This work was supported by the Russell Berrie Nanotechnology Institute at the Technion-Israel Institute of Technology (T.M.), and by the James Frank and Wolfson Foundations at Tel-Aviv University (S.R.).

[1] T. W. Ebbesen, H. J. Lezec, H. F. Ghaemi, T. Thio, and P. A. Wolff, Nature (London) **391**, 667 (1998).
[2] C. Genet and T. W. Ebbesen, Nature (London) **445**, 39 (2007).
[3] Z. Sun and H. K. Kim, Appl. Phys. Lett. **85**, 642 (2004).
[4] B. Leca-Bouvier and L. J. Blum, Anal. Lett. **38**, 1491 (2005).
[5] F. J. Garcia-Vidal, L. M. Martic-Moreno, T. W. Ebbesen, and L. Kuipers, Rev. Mod. Phys. **82**, 729 (2010).
[6] Y. Ding, J. Yoon, M. H. Javed, S. H. Song, and R. Magnusson, IEEE Phot. Jour. **3**, 365 (2011).
[7] P. E. Batson, Ultramicroscopy **11**, 299 (1983).

[8]H. Cohen, T. Maniv, R. Tenne, Y. Rosenfeld Hacohen, O. Stephan, and C. Colliex, Phys. Rev. Lett. **80**, 782 (1998).
[9]J. Nelayah, M. Kociak, O. Stéphan, F. J. G. de Abajo, M. Tencé, L. Henrard, D. Taverna, I. Pastoriza-Santos, L. M. Liz-Marzán, and C. Colliex, Nat. Phys. **3**(5), 348 (2007).
[10]W. Sigle, J. Nelayah, C. T. Koch, and P. A. van Aken, Opt. Lett. **34**(14), 2150 (2009).
[11]F. J. G. de Abajo, Rev. Mod. Phys. **82**, 209 (2010).
[12]N. Zabala, A. G. Pattantyus-Abraham, A. Rivacoba, F. J. García de Abajo, and M. O. Wolf, Phys. Rev. B **68**, 245407 (2003).
[13]M. A. Itskovsky, H. Cohen, and T. Maniv, Phys. Rev. B **78**, 045419 (2008).
[14]I. Carmeli, M. A. Itskovsky, Y. Kauffmann, Y. Shaked, S. Richter, T. Maniv, and H. Cohen, e-print arXiv:1105.3711v1.
[15]Z. I. Wang, Micron **27**, 265 (1996).
[16]Shin-Hui Chang, S. K. Gray and G. C. Schatz, Opt. Express **13**, 3150 (2005).
[17]E. Verhagen, L. Kuipers, and A. Polman, Opt. Express **17**, 14586 (2009).
[18]R. Gordon and A. G. Brolo, Opt. Express **13**, 1933 (2005).